SCIENCE CHINA
Chemistry

• REVIEWS •

Structural Tailoring of Covalent Organic Frameworks with Steric Effects

Guiqing Lin[1†], Arindam Mal[1†], Xuejiao Wang[1], Xu Zhou[1], Bo Gui[1] & Cheng Wang[1*]

[1] *College of Chemistry and Molecular Sciences, Wuhan University, Wuhan 430072, China*

Received ***; accepted ***; published online ***

Covalent organic frameworks (COFs) provide a unique platform with tunable structures allowing precise control of pore sizes, shapes and functions. The key to synthesizing COFs with desired structures is to precisely control the conformation and geometry of building blocks as well as the growth direction of COFs. To achieve this, steric effects are noteworthy that may have a significant impact on the assembly of COFs. Specifically, the introduction of sterically demanding substituents or bulky groups into monomers of COFs will lead to intramolecular conformational changes and intermolecular repulsions, which induce structural changes of COFs, including changes in torsion angles, interlayer distances, stacking modes and topologies of 2D COFs, and changes in spatial nodes, interpenetration and topologies of 3D COFs. This review will help to understand the impacts of steric effects on the structures of COFs and to take them into extensive considerations in the design and synthesis of COFs with novel functionalities and structural attributes.

Covalent organic frameworks, steric effect, structural tailoring

Citation: Lin G, Mal A, Wang X, Zhou X, Gui B, Wang C. Structural Tailoring of Covalent Organic Frameworks with Steric Effects. *Sci China Chem*, ***, doi: ***

1 Introduction

Covalent organic frameworks (COFs) [1] are a novel class of porous crystalline materials constructed from covalently linked organic molecules that are assembled into two-dimensional (2D) stacked layers or cross-linked three-dimensional (3D) networks. COFs provide a unique platform with tunable structure allowing precise control of pore size, shape and functionality, offering the opportunity to tailor their properties for specific applications, such as gas storage and separation [2], catalysis [3], sensing [4], optoelectronics [5], etc. Therefore, since the first report in 2005 [6], constant efforts have been made to diversify the structure and function of COFs by introducing new building blocks [7], topologies [8], linkages [9], synthetic methods [10], etc.

The successful construction of COFs is achieved through a mesh of appropriate monomers which are strategically designed and encoded to amplify desired structural and functional properties. Thus, the key to expanding the family of COFs with preferred structures and topologies is to precisely control the steric impact of building blocks with different conformations and geometries. Specifically, the introduction of substituents with steric requirements in organic precursors brings about conformational changes (e.g., torsion angles) in the building blocks [11] and further significantly affects the reticular structure and crystal growth orientation of COFs, as spatially close groups cause intramolecular strains and intermolecular repulsions. Moreover, steric repulsion between building blocks may disrupt the interaction of layers in 2D COFs and networks in 3D COFs,

†These authors contributed equally to this work.

*Corresponding authors (email: chengwang@whu.edu.cn)

leading to noteworthy structural changes (e.g., stacking mode, interpenetration degree) in COFs [12], even achieving unprecedented topologies [13]. Furthermore, steric effects caused by bulky substituents can hinder the accessibility of reactive sites or slow down the reaction kinetics, making it more challenging to achieve highly crystalline COFs, affecting the ordering of COF structures, and leading to variations in porosity and surface area [14]. Overall, understanding and controlling the steric factors is essential for the design and synthesis of COFs with novel functionalities and structural attributes.

In the field of COF research, although a considerable number of interesting review articles have been published, a systematic and brief discussion regarding the impacts of steric effects on the design and synthesis of COFs is still very limited. In this mini review, we will focus on how steric effects can be an important tool for the structural diversification of 2D and 3D COFs. By showing representative examples and discussing the structural changes of COFs while incorporating substituents with steric requirements into building blocks, we wish to highlight steric effects into extensive considerations for the design and synthesis of functional COFs and to promote application of COFs with steric effects. Finally, as part of the concluding remarks, an outlook on the future challenges and prospects of this field will be covered.

2 Steric Effects on Structural Changes of 2D COFs

The sterically hindered substituents in building blocks impart a profound impact on the reticulation and the resulting extended layered structure formation in 2D COFs. The intra- or inter-molecular repulsions induced by bulky functional groups alter the torsion angles of peripheral units [11a, 15]. This leads to disruption of layer stacking, resulting in an increase of the interlayer distance [16] and even altering the stacking mode [12a, 17] or topology of 2D COFs [18]. As a result, longer side chains and larger substituents generally reduce the crystallinity and porosity of 2D COFs [14].

2.1 Torsion angle changes

Steric repulsions between substituted groups and adjacent units cause conformational changes, especially rotations and torsion angle changes of neighboring rings in 2D COFs, which greatly affect the planarity and conjugation of the frameworks.

In a typical example, Lotsch and co-workers [11a] substituted the C-H moiety in the central phenyl ring of triphenylbenzene by N atoms and synthesized a series of 2D azine-linked N_x-COFs where x is the number of N in the central aryl ring (x = 0, 1, 2 and 3) (Figure 1a and b). As the number of replaced N atoms increased, the torsion angle between the central aryl ring and the adjacetn phenyl rings decreased on account of the decrease in steric repulsions according to density functional theory (DFT) calculations (Figure 1c-f), further improving the planarity and crystallinity of COFs. Upon investigating N_x-COFs as a photocatalyst, the photocatalytic hydrogen evolution properties enhanced progressively with the number of N atoms in triphenylaryl core.

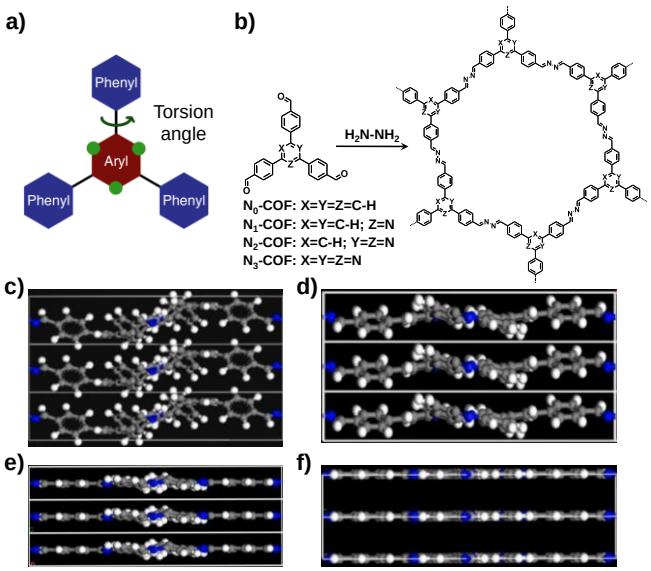

Figure 1 a) Representation of torsion angle changes in triphenylaryl platform. Substituting 'C–H' with 'N atoms' at the green dots brings about the torsion angle changes between central aryl and peripheral rings. b) Synthesis of N_x-COFs from N_x-aldehydes and hydrazine (x = 0, 1, 2 and 3). Side views of simulated structures of c) N_0-COF, d) N_1-COF, e) N_2-COF, and f) N_3-COF [11a].

In another work, Kuo, Kim and co-workers [19] synthesized TPA-COFs and TPT-COFs through one-pot polycondensations of triarylamines [tris(4-aminophenyl)amine (TPA-3NH_2) and 2,4,6-tris(4-aminophenyl)triazine (TPT-3NH_2)] with triarylaldehydes. When the central units of monomers changed from N atom and pyridine to triazine, the torsion angles between peripheral aryl rings decreased, resulting in COFs with higher degree of planarity and crystallinity. Moreover, the integration of the triaryltriazine unit with higher planarity and more nitrogen atoms into the skeleton of the TPA-COFs and TPT-COFs significantly influences the interactions with CO_2, leading to higher CO_2 uptakes. Considering the potential application of COFs in radioactive iodine waste capture, Zeng, Liu, Zhao and co-workers [20] synthesized two COFs (TJNU-201 and TJNU-202) by reticulating a twisted 3-connected building block 1,3,5-trimethyl-2,4,6-tris(4-aminophenyl)-benzene with sterically demanded methyl groups. The structural analysis of both COFs showed that owing to the steric hindrance of methyl groups, imine bonds and phenyl rings connected to them were aligned almost vertically to the lay-

ers of 2D COFs and more exposed towards the pores making them more suitable for guest adsorption. As a result, ultrahigh iodine capture capacity (5.625 g g^{-1} for TJNU-201 and 4.820 g g^{-1} for TJNU-202) was achieved due to the physical-chemical adsorption. Recently, Du *et al.* [15c] constructed a series of isostructural 2D COFs by applying triphenylbenzene- and triphenyltriazine-based C_3-symmetric monomers. The theoretical studies showed that when the central triazine units were replaced by benzene, the torsion angle between central and peripheral rings increased from 0° to 31.4°, disturbing the planarity of 2D COFs and forming propeller-like structure, thus weakening the interlayer interaction. Compared with non-triazine COFs, the highly crystalline triazine-core-based COFs with planar and rigid triazine units displayed 10 times higher proton conductivity of 1.27×10^{-2} S cm^{-1} at 160 °C.

In addition to 3-connected triphenylaryl based monomers, torsion angles caused by steric hindrance in 4-connected units are also systematically investigated. In an early study, Bein's group [15a] prepared a series of pyrene-based 2D COFs, and found that the steric repulsions between the hydrogens in the core tetraphenylpyrene unit forced phenyl to rotate against pyrene. As a result, the tetraphenylpyrene core formed the "armchair" conformation inducing synchronized slipped stacking in 2D COFs for less offset and closer packing, rather than the "propeller" conformation in the model compound. The controlled geometry of tetraphenylpyrene-derived building block produced a periodic lattice of synchronized docking sites which allowed the growth of highly crystalline 2D COFs with domain sizes of half a micrometer. Detailed optoelectronic experiments suggested these highly crystalline features contributed to extensive electron delocalization across the π-stacked central tetraphenylpyrene core and connecting units. Later, Bein, Auras and co-workers [15b] incorporated isoindigo- and thienoisoindigo-based monomers as bridges into highly crystalline imine-linked COFs (Py-pII, Py-pTII and Py-tTII) with tetraphenylpyrenes as a node, respectively. In the case of Py-pII and Py-pTII, steric repulsion between phenyl and isoindigo or thienoisoindigo led to rotation of the bridge, but in Py-tTII, the repulsion was replaced by electrostatic attraction, making the bridge more planar. In another case, Bein, Auras *et al.* [21] synthesized a series of imine-linked 2D COFs by co-condensation of 1,1,2,2-tetrakis(4-aminophenyl)ethene and linear dialdehydes. Theoretical analysis and comparison with the model compound revealed that tetraphenylethene units adopted a propeller-like conformation in the COFs due to the repulsions between aromatic rings, where the twist angle was around 44°.

2.2 Interlayer distance and exfoliation

Since sterically demanded groups in building blocks interfere the interlayer stacking in 2D COFs, the supramolecular interactions (π-π stacking, hydrogen bonding, etc.) operated between COF layers are weakened, resulting in an increased interlayer distance. If the interactions are too weak to maintain layered stacking structures, 2D COFs with steric effects can be easily exfoliated into covalent organic nanosheets.

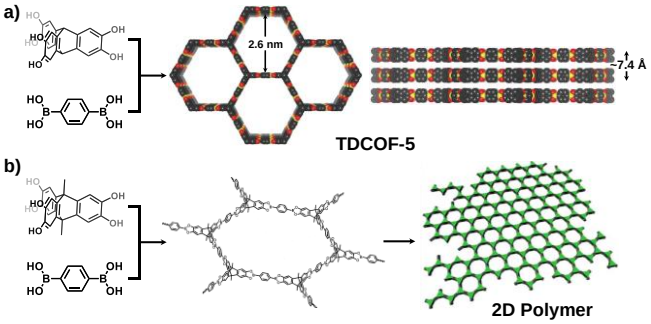

Figure 2 a) Synthesis of TDCOF-5 and space-filling models showing solid-state (AA) stacking: top-view (left) and side-view (right) [22]. b) Synthesis of triptycene-based 2D polymeric monolayers [23].

El-Kaderi and co-workers [22] have reported the synthesis of boronate ester-linked TDCOF-5 by condensation of hexahydroxytriptycene and 1,4-benzenediboronic acid. The structural analysis illustrated that triptycene core was aligned perpendicularly to the 2D COF plane, exhibiting a large interlayer *d*-spacing value of 7.4 Å due to the non-planar conformation of triptycene units (Figure 2a). In the same year, Zhao and co-workers [23] introduced two steric methyl groups into 9,10-positions of hexahydroxytriptycene to suppress interlayer interactions and synthesized 2D polymeric monolayers without aggregating in solution (Figure 2b). As the polymerization degree became higher, the monolayers were found to curl and evolve into hollow spheres.

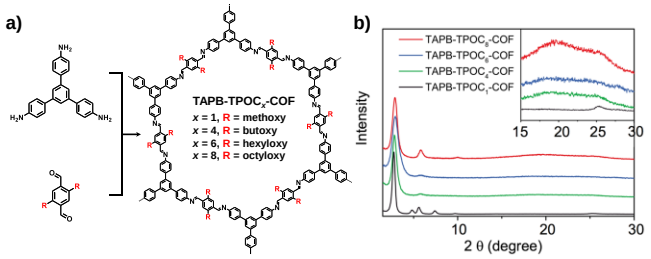

Figure 3 a) Synthesis and chemical structures of TAPB-TPOC$_x$-COF films (x = 1, 4, 6, and 8). b) Comparison of the experimental PXRD patterns of TAPB-TPOC$_x$-COF films (x = 1, 4, 6 and 8). Inset is the enlargement of the peaks assigned to (001) planes [16a].

In general, for 2D COFs, the peaks of powder X-ray diffraction (PXRD) patterns assigned to the (001) planes reflect the π-π stacking and interlayer distance. Wang, Feng and co-workers [16a] proposed the synthesis of flexible TAPB-TPOC$_x$-COF films (x = 1, 4, 6 and 8) via interfacial polymerization of 1,3,5-tris(4-aminophenyl)benzene and terephthalaldehyde with dialkoxy substituent (methoxy,

butoxy, hexyloxy, and octyloxy) (Figure 3a). Based on PXRD patterns, the peaks of (001) planes became broad and shifted to lower angles as alkoxy chain length increased (Figure 3b). Simulation results revealed that the longer alkoxy side chain loosened the layered stacking by increasing the interlayer distance and distorting the planar structure.

Chen, Xu and co-workers [16b] also observed the shift of PXRD peaks assigned to (001) planes after introducing substituted groups. The co-condensation reaction of 4,4',4'',4'''-(pyrene-1,3,6,8-tetrayl)tetrabenzaldehyde with thiadiazole-based diamines substituted by H, F and Cl atoms yielded Py-*X*TP-BT-COFs (*X* = H, F, Cl), respectively. PXRD measurements of the COFs exhibited that the peaks of (001) planes were found to be 23.46° (Py-HTP-BT-COF), 23.27° (Py-FTP-BT-COF) and 23.14° (Py-ClTP-BT-COF). This suggested that interlayer distances in Py-FTP-BT-COF and Py-ClTP-BT-COF were increased compared with Py-HTP-BT-COF due to larger steric hindrance of F and Cl atoms. In addition, the optimized structures and unit cell parameters presented that the *c* axis values of Py-FTP-BT-COF and Py-ClTP-BT-COF were larger than that of Py-HTP-BT-COF due to the steric impact of F and Cl atoms. Recently, Jiang, Zhao *et al*. [16c] constructed a series of isostructural porphyrin-based COFs (COFX, X = 1–5) among which COF5 with steric pentafluorobenzene group at proximal position showcased a π-π stacking peak at 25.0°, which was lower than the COFs with unmodified porphyrin units.

Smaldone *et al.* [24] reported how side chains affected the crystallinity and interlayer distances of 2D COFs. Tritopic aldehyde was modified with methyl groups and long amide chains, and further condensed with 4,4′-(pyrene-2,7-diyl)dianiline to produce polymer and PyCOFamide, respectively. The polymer exhibited amorphous structure due to pore collapse or poor interlayer stacking. However, PyCOFamide showed high crystallinity due to interlayer hydrogen bonding between amide units, and a (001) reflection peak at 18.5°, indicating an increased interlayer distance (~4.8 Å) caused by the steric hindrance of amide chains and rotating phenyl rings.

With further increase in steric hindrance, the layer-to-layer interactions will be weaker, which may lead to the exfoliation of COFs. Banerjee's group [25] reported a strategy to delaminate anthracene-based 2D COF DaTp into covalent organic nanosheets (CONs) by chemical functionalization with large steric group N-hexylmaleimide. The anthracene units in DaTp reacted with N-hexylmaleimide through Diels-Alder cycloaddition reaction, resulting in the distortion of anthracene units and the attachment of large steric groups to the layers, thus facilitating the exfoliation of DaTp. Recently, Loh *et al*. [26] designed and synthesized two crown ether integrated monomers, CyHz1 (two dihydrazides forming a crown ether macrocycle) and CyHz0 (dihydrazide with crown ether) to construct MCOF-1 and MCOF-0, respectively. MCOF-0 exhibited a broad peak at 24.87°, which was lower than that of MCOF-1 (26.2°), indicating an increased interlayer distance in MCOF-0 due to disrupted stacking and steric hindrance compared to π-π interactions and hydrogen bonding-assisted stacking of CyHz1 in MCOF-1. Further, the complexation of methyl viologen into the crown ether macrocycles of MCOF-1 and MCOF-0 generated pseudorotaxane COFs that exfoliated into monolayers due to electrostatic repulsion.

2.3 Stacking mode

One of the important aspects in the crystallization process of 2D COFs is the stacking of extended layers through non-covalent interactions. Thus, steric factors induce a profound impact on the stacking mode of 2D COFs. In general, steric interactions between substituted groups cause offsets of adjacent layers in 2D COFs. Once the steric groups or steric repulsions are too large, the stacking mode of 2D COFs may change from AA to AB, or even ABC stacking to weaken the repulsions and stabilize the frameworks.

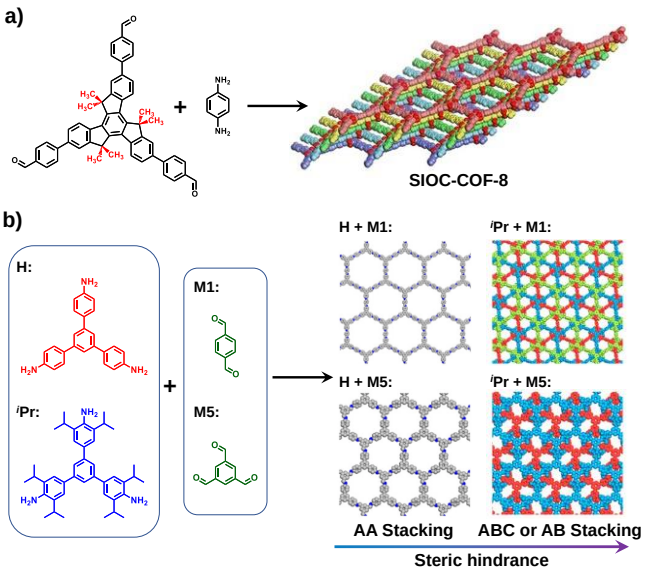

Figure 4 a) Synthesis of SIOC-COF-8 with inclined stacking mode [17b]. b) Schematic representation of controlling the stacking modes of 2D COFs via steric tuning [12a].

In 2017, Zhao *et al*. [17b] presented a case study on how steric substitutes influenced the stacking mode of 2D COFs. The authors reticulated a modified truxene derivative with methyl groups, 3,8,11-tri(4-formylphenyl)-5,5,10,10,15,15-hexamethyltruxene, with 1,4-diaminobenzene and benzidine to afford SIOC-COF-8 (Figure 4a) and SIOC-COF-9, respectively. The results revealed that both COFs adopted inclined stacking mode with adjacent layers offset by 8.2 Å, instead of AA stacking, due to the steric hindrance of methyl groups. Cui and co-workers [27] constructed N,N-diaryl dihydro-

phenazine (PN)-based COFs by reacting 5,10-di(3,5-diformylphenyl)-5,10-dihydrophenazine with linear diamines. All the 2D COFs exhibited slipped AA stacking mode due to the steric repulsions of PN units. The PN units in the 2D COFs were aligned perpendicularly to the layers to some extent, causing an offset of 3.7-3.9 Å between PN units in adjacent layers.

Cui, Liu *et al*. [12a] reported the control of stacking mode of 2D COFs by tuning the steric groups in monomers (Figure 4b). 1,3,5-Tris(4-aminophenyl)benzene (**H**) was chosen and modified with ethyl and isopropyl groups to give steric monomers **Et** and **^{i}Pr**, respectively, and further reacted with di- or trialdehydes to afford 2D COFs. The 2D COFs synthesized from **H** and di- or trialdehydes exhibited AA stacking mode. However, due to the steric hindrance of alkyl substituents, the 2D COFs produced by **Et** and **^{i}Pr** with linear dialdehydes exhibited ABC stacking mode, while the 2D COFs generated from **Et** and **^{i}Pr** with trialdehydes featured AB stacking mode. Moreover, in multivariate (MTV) COFs, higher ratios of **Et** and **^{i}Pr** with alkyl substituents produced 2D COFs adopting AB or ABC stacking mode, while higher concentration of **H** without substituents led to 2D COFs with AA stacking mode.

Zamora *et al*. [28] applied molecular steric engineering to control the stacking mode and solid-state photoluminescence of 2D imine-linked COFs (IMDEA-COF-1 and -2) constructed by reacting 1,3,5-benzenetricarbaldehyde (BTCA) and 2,4,6-triformylphloroglucinol (TFP) with 1,6-diaminopyrene (DAP), respectively. PXRD patterns and computational modeling revealed that IMDEA-COF-1 had an AB stacking mode, while IMDEA-COF-2 showed an AA stacking structure. The steric repulsions between pyrene units, hydroxyl groups and imine bonds forced the formation of planar layers and led to AA stacking of IMDEA-COF-2. Moreover, the difference in layer packing resulted in significant variation in the arrangement of the pyrene units of IMDEA-COFs, leading to different layer-packing-driven solid-state fluorescence of IMDEA-COFs. IMDE-COF-1 with eclipsed stacking exhibited green emission in the solid state with an absolute emission quantum yield value of 3.5%, while IMDEA-COF-2 was non-fluorescent under UV irradiation.

Yin *et al*. [29] demonstrated the steric effects of side chains on stacking modes of 2D COFs. COF-0-OH and COF-4-OH were prepared by co-condensation of TFP with 2,7-diaminofluorene and 9,9-dibutyl-2,7-diaminofluorene, respectively. COF-0-OH was found to have an AA stacking mode, while COF-4-OH exhibited an AB stacking mode owing to the steric hindrance of long *n*-butyl chains. Seki *et al*. [17a] described the synthesis of 2D COFs from the condensation of TFP and linear diamines with different steric groups, including benzene (TP), anthracene (Ant), benzothiadiazole (Bt) and tetrazine (Tz). The torsion angles in diamines increased as the steric groups became larger, resulting in 2D COFs with AB or ABC stacking mode. In addition, higher reaction temperatures led to the COFs with slipped AA or AB stacking.

Cui's group [30] reported the synthesis of 2D chiral COFs (CCOFs) by reacting sterically large monomer tetraaryl-1,3-dioxolane-4,5-dimethanols (TADDOLs) with 4,4'-diaminodiphenylmethane (4,4'-DADPM). Subsequent PXRD, theoretical calculations and pore size distribution analyses confirmed that CCOF-1 adopted an unusual two-fold interpenetrated net with AB stacking mode, while CCOF-2 possessed a non-interpenetrated net with AB stacking mode. Recently, they have incorporated a chiral diphosphine ligand (R)-MeO-BIPHEPA with large steric hindrance into 2D CCOFs [31]. Due to the steric effects of (R)-MeO-BIPHEPA, a quarter of the aldehydes in the diphosphine ligand were retained during the condensation process, and the CCOFs showed ABC stacking mode. Apart from imine-linked COFs, 2D olefin-linked COFs with ABC stacking mode were also constructed. Narita *et al*. [32] have employed C_2-symmetric dibenzo[*hi*,*st*]ovalene (DBOV)-based DBOV-CHO and 3,5-dicyano-2,4,6-trimethylpyridine (DCTMP) as building blocks to synthesize a -C=C- linked 2D DBOV-COF that exhibited ABC stacking due to the large steric hindrance of methyl groups. As a result, active sites of DBOV-COF are more accessible for interacting with external guest molecules.

2.4 Topologies of 2D COFs

Building blocks with steric substituents also induce topological changes in 2D COFs. In case the expected topology-guided 2D COFs lack enough space to accommodate steric groups in pores, the topology may change to overcome steric repulsions and form COFs with other topologies.

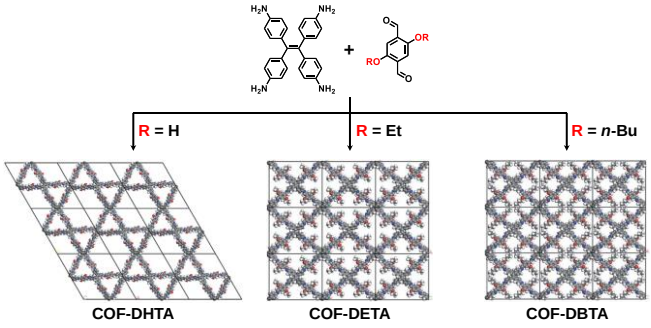

Figure 5 Synthesis and structures of a dual-pore COF (COF-DHTA) and single-pore COFs (COF-DETA and COF-DBTA) from ETTA and dialdehyde with different substituents (H = hydrogen atoms, Et = ethyl groups, *n*-Bu = *n*-butyl groups) [18].

Zhao and co-workers [18] reported the first topological regulation of 2D COFs by introducing steric substituents. COF-DHTA with hydroxyl groups constructed from 2,5-dihydroxyterephthalaldehyde (DHTA) and

4,4',4'',4'''-(ethene-1,1,2,2-tetrayl)tetraaniline (ETTA), presented a kagome dual-pore topology. However, COF-DETA and COF-DBTA built from 2,5-diethoxyterephthalaldehyde (DETA) and 2,5-dibutoxyterephthalaldehyde (DBTA) with ETTA, respectively, exhibited a rhombus-like single-pore topology (Figure 5) in order to reduce steric repulsions between long alkyl chains.

Deng and co-workers [33] presented the topological regulation of 2D COFs by applying steric organic Lewis acid tris(pentafluorophenyl)borane (TPFB) as catalyst. The authors obtained COF-820 with **sql** topology and quadrilateral pores through the condensation of ETTA and terephthalaldehyde under catalyzed by TPFB. However, in contrast, the same building blocks under Brønsted acid catalysis afforded 4PE-1P-COF with **kgm** topology, because the steric size of TPFB was larger than the triangular pore in 4PE-1P-COF. In addition, using aniline as a quencher of TPFB, a mixed phase appeared with increasing aniline dosage, and the phase corresponding to **sql** topology decreased gradually.

3 Steric Effects on Structural Changes of 3D COFs

In contrast to 2D COFs, the design and synthesis of 3D COFs are considered to be very challenging [34]. As a result, controlling steric factors of the building blocks is crucial to the successful construction of 3D COFs with tailored structural features [11b]. The monomers with sterically demanding substituents upon extended reticulation and subsequent 3D network formation results into altered folds of interpenetration [12b, 35], appearance of unprecedented topology [13] etc.

3.1 Constructing spatial nodes

The primary criterion for constructing 3D COFs is to select molecular node that can be reticulated in spatial directions. In general, non-planar tetrahedral building blocks are preferred choices [10e, 36]. However, the integration of steric substituents into planar molecules induces an increased torsion angle and strain between neighboring units, leading to conformational changes of the molecules and the formation of non-planar spatial nodes.

In this regard, Wang, Sun and co-workers [11b] introduced a biphenyl-based monomer with methyl groups positioned in sterically demanding position and constructed a new tetrahedral node for 3D COFs (Figure 6). The authors reversibly condensed 3,3',5,5'-tetra(*p*-aminophenyl)-biphenyl (BPTA) and 3,3',5,5'-tetra(*p*-aminophenyl)-bimesitylene (BMTA) with 1,2,4,5-tetrakis(4-formylphenyl)-benzene (TPB-H) to give two COFs, respectively. According to the crystal structures resolved from continuous rotation electron diffraction (cRED), for BPTA without methyl groups, the dihedral angle between the biphenyl rings was around 0° in the framework due to negligible steric interactions, leading to the formation of a 2D COF (2D-BPTA-COF). However, for BMTA with methyl groups at the ortho positions of biphenyl rings, the dihedral angle between the biphenyl core was restricted to 60° in the framework due to the large steric repulsions, forcing BMTA to form a tetrahedral conformation and producing a 3D COF (3D-BMTA-COF) with 7-fold interpenetrated **pts** topology.

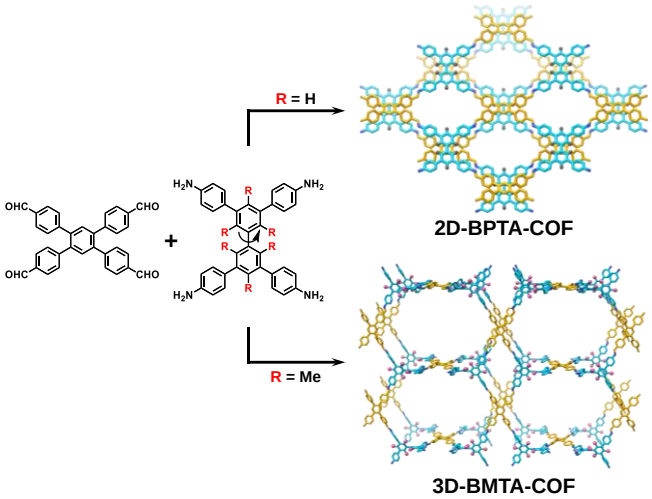

Figure 6 Schematic representation of the synthesis of 2D-BPTA-COF and 3D-BMTA-COF based on biphenyl units through steric tuning (H = hydrogen atoms, Me = methyl groups) [11b].

One of the main obstacles for diversifying 3D COFs is the availability of suitable nodes. Therefore, in past few years, constant efforts have been made to construct 3D COFs by applying high valency nodes through new topology directed designs. Zhang and co-workers [37] demonstrated the significant influence of steric factors to develop an 8-connected stereoscopic node for the construction of 3D COFs. The synthesized 8-connected node, 4',5'-bis(3,5-diformylphenyl)-3',6'-dimethyl-[1,1':2',1''-terphenyl]-3,3'',5,5''-tetracarbaldehyde (DPTB-Me), showed a cuboid shape owing to the steric hindrance of two methyl groups on the central phenyl ring, which made a dihedral angle of about 75° between central and peripheral rings, forcing the molecule to form the desired spatial conformation. A series of 8-connected 3D COFs (NKCOF-21, -22 and -23) with **bcu** topology were obtained by the co-condensation of DPTB-Me and linear diamines. Peng, Zhu, Dai *et al.* [38] reported another 8-connected node, 1,3,6,8-tetrakis 3,5-bis[(4-amino)phenyl]phenylpyrene (OAPy) exhibiting D_{4h} symmetry due to steric hindrance and reacted with diamines to afford 3D COFs (ZJUT-2 and ZJUT-3) with 2-fold interpenetrated **bcu** topology. Similarly, Fang, Yao, Li *et al.* [39] synthesized two 8-connected building blocks,

3,3’,5,5’-tetra(3’’,5’’-diformylphenyl)-2,2’,6,6’-tetramethoxy-4,4’-dimethyl biphenyl (TDFTD) and 2,3,5,6-tetrakis(([3,5-diformylphenyl]-5-yl)-9*H*-carbazol-9-yl)-1,4-benzenedicarbonitrile (TDFCB). Due to steric hindrance, both TDFTD and TDFCB displayed cubic geometry, which were condensed with 1,4-phenylenediamine to give 3D COFs, JUC-588 and JUC-599, respectively, with **bcu** topology.

3.2 Interpenetration degree

In the construction process of 3D COFs, interpenetration helps in managing the vacant space and stabilizes the overall network. It has been generally noticed with the longer struts [40]. Moreover, highly interpenetrated 3D COFs were built with micropore apertures and smaller pore volume [41]. Introducing substituents with steric demands into building blocks will increase intermolecular repulsions during the assembly of 3D COFs. In order to reduce these unfavorable interactions, the building blocks with steric groups will tend to accommodate into the framework with fewer folds of interpenetration and highly accessible pores.

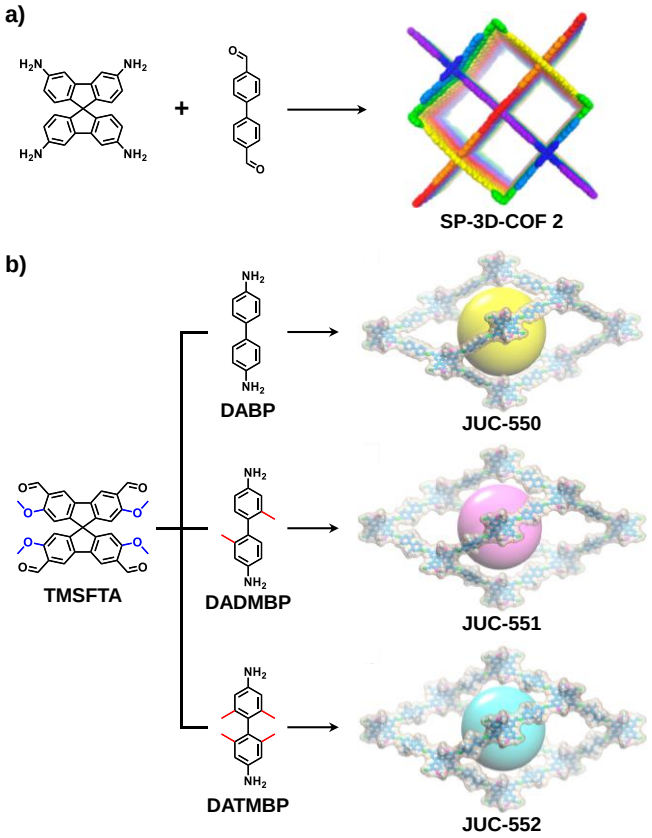

Figure 7 a) Synthesis and structure of SP-3D-COF 2 with high interpenetration degree [42]. b) Synthesis of JUC-550 to -552 by the condensation reaction of TMSFTA and DABP, DADMBP, or DATMBP, and the non-interpenetrated **dia** structures of JUC-550 to -552 [12b].

Zhao, Li, Jiu *et al.* [42] selected 3,3’,6,6’-tetraamine-9,9’-spirobifluorene with tetragonal-disphenoid conformation as the tetrahedral node and condensed with linear dialdehydes to synthesize SP-3D-COFs featuring microporous structures with high interpenetration degrees (Figure 7a). Later, Fang and co-workers [12b] introduced multiple methoxy groups into spirobifluorene core and selected biphenyl units with methyl groups to synthesize non-interpenetrated 3D COFs. Methoxy-modified 2,2’,7,7’-tetramethoxy-9,9’-spirobi[fluorene]-3,3’,6,6’-tetracarbaldehyde (TMSFTA) was synthesized and condensed with 4,4’-diaminobiphenyl (DABP), 4,4’-diamino-2,2’-dimethylbiphenyl (DADMBP) and 4,4’-diamino-2,2’,6,6’-tetramethylbiphenyl (DATMBP) to produce 3D COFs (JUC-550, JUC-551 and JUC-552), respectively. Due to the steric hindrance of methoxy and methyl groups, all the 3D COFs featured mesoporous structures with non-interpenetrated **dia** topology (Figure 7b) and high specific surface area.

In another case, Fang and co-workers [35] chose tetrakis(3-formyl-4-hydroxylphenyl)methane (TFHPM) as the tetrahedral node and 4,5-difluorophenylene-1,2-diamine (DFPDA), 4,5-dichlorophenylene-1,2-diamine (DCPDA) as linkers to synthesize 3D Salphen-based COFs (JUC-508 and JUC-509), respectively. The subsequent PXRD measurements combined with theoretical simulations revealed that both 3D COFs possessed non-interpenetrated **dia** networks owing to the steric hindrance of Salphen units.

3.3 Topologies of 3D COFs

The topology design strategies for constructing 3D COFs were found to be highly dependent on steric factors induced by bulky substituents in building blocks. In the process of minimizing intermolecular steric repulsions, building blocks with different steric bulk may produce 3D COFs with altered topology under the same construction approach.

In 2021, Wang, Sun and co-workers [13] reported for the first time the topology tuning of 3D COFs through steric control (Figure 8). Tetraphenylbenzene core with different steric substituents (methoxy and phenyl) were selected as quadrilateral building blocks (TPB-OMe and TPB-Ph) for subsequent condensation with the tetrahedral node tetra(*p*-aminophenyl)-methane (TAPM) and generated 3D-TPB-COF-OMe and 3D-TPB-COF-Ph, respectively. The crystal structures analyses using cRED technique showed that 3D-TPB-COF-OMe possessed 5-fold interpenetrated **pts** topology, which was identical to other 3D-TPB-COFs with H, F, methyl, or hydroxyl substituents, indicating the steric hindrance of methoxy groups was not sufficient to change the topology. However, due to the large steric repulsions of phenyl groups, 3D-TPB-COF-Ph crystallized in unprecedented **ljh** topology with a self-interpenetrated net. Later, BMTA was used instead of TAPM as elongated tetrahedral node to produce

3D-BMTA-COF-Ph with the targeted **pts** topology [43]. The extended shape of BMTA led to increased intermolecular distance between TPB-Ph units in the framework, which alleviated the intermolecular repulsions and promoted the formation of 3D-BMTA-COF-Ph with 5-fold interpenetrated **pts** topology.

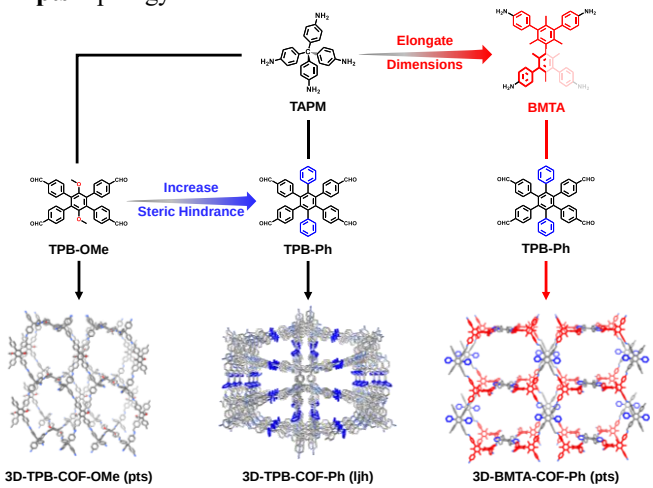

Figure 8 Schematic representation of the synthesis and topology tuning of 3D-TPB-COF-OMe, 3D-TPB-COF-Ph and 3D-BMTA-COF-Ph through steric control [43].

4 Conclusions and outlooks

In conclusion, steric effects play an important role in tailoring the structures of COFs. Introducing sterically demanding substituents or bulky groups into monomers brings about conformational changes and intermolecular repulsions of building blocks, thus leading to structural changes of COFs. For 2D COFs, the steric substituents generally affect the torsion angles between adjacent units, disrupt the planarity and π-π stacking of layers, and lead to increased interlayer distances or, if the steric hindrance is too high, changes in stacking mode and topology of the framework. For 3D COFs, the incorporation of steric groups may force the monomers to form spatial nodes with stereoscopic conformation, reduce the degree of interpenetration of 3D COFs and even induce the formation of new frameworks with altered topologies.

Although great progress has been made in studying steric effects on the structural changes and tailoring of COFs, there are still many aspects to be investigated. Understanding the steric effects and structure-property-function relationship largely relies on the precise structures of COFs, which remains a great challenge in the field of COFs. In addition, systematic investigations on the steric effects affecting the structures of COFs are still deficient, such as in what cases would the substituents with steric requirements induce the formation of new frameworks with altered topology, rather than changing the stacking modes or reducing the degree of interpenetration. Moreover, the targeted synthesis of COFs with desired spatial conformations and topologies is still limited, thus the applications based on steric effects in COFs have not been well explored.

Overall, understanding the impacts of steric effects on the structures of COFs will provide deep insight into the design and synthesis of COFs with desired structures and functionalities, and promote the explorations of structure-property-function relationships and applications of COFs.

Acknowledgments This work was supported by the National Natural Science Foundation of China (22225503, U21A20285, 21975188, 22105149). G.L. acknowledges the financial support from the fellowship of China National Postdoctoral Program for Innovative Talents (BX2021226).

Conflict of interest The authors declare that they have no conflict of interest.

1 a) Liu, R; Tan, KT; Gong, Y; Chen, Y; Li, Z; Xie, S; He, T; Lu, Z; Yang, H; Jiang, D. *Chem Soc Rev*, 2021, 50: 120–242; b) Diercks, CS; Yaghi, OM. *Science*, 2017, 355: eaal1585; c) Ding, SY; Wang, W. *Chem Soc Rev*, 2013, 42: 548–568; d) Gui, B; Ding, H; Cheng, Y; Mal, A; Wang, C. *Trends Chem*, 2022, 4: 437–450; e) Guan, X; Chen, F; Fang, Q; Qiu, S. *Chem Soc Rev*, 2020, 49: 1357–1384.

2 a) Li, J; Cheng, Z; Wang, Z; Dong, J; Jiang, H; Wang, W; Zou, X; Zhu, G. *Angew Chem Int Ed*, 2023, 62: e202216675; b) Wang, S; Yang, Y; Liang, X; Ren, Y; Ma, H; Zhu, Z; Wang, J; Zeng, S; Song, S; Wang, X; Han, Y; He, G; Jiang, Z. *Adv Funct Mater*, 2023, 33: 2300386; c) Zhang, Z; Kang, C; Peh, SB; Shi, D; Yang, F; Liu, Q; Zhao, D. *J Am Chem Soc*, 2022, 144: 14992–14996; d) Jin, F; Lin, E; Wang, T; Geng, S; Hao, L; Zhu, Q; Wang, Z; Chen, Y; Cheng, P; Zhang, Z. *J Am Chem Soc*, 2022, 144: 23081–23088; e) Zhao, S; Jiang, C; Fan, J; Hong, S; Mei, P; Yao, R; Liu, Y; Zhang, S; Li, H; Zhang, H; Sun, C; Guo, Z; Shao, P; Zhu, Y; Zhang, J; Guo, L; Ma, Y; Zhang, J; Feng, X; Wang, F; Wu, H; Wang, B. *Nat Mater*, 2021, 20: 1551–1558.

3 a) Yang, H; Hao, M; Xie, Y; Liu, X; Liu, Y; Chen, Z; Wang, X; Waterhouse, GIN; Ma, S. *Angew Chem Int Ed*, 2023: e202303129; b) Kan, X; Wang, JC; Chen, Z; Du, JQ; Kan, JL; Li, WY; Dong, YB. *J Am Chem Soc*, 2022, 144: 6681–6686; c) Wang, LK; Zhou, JJ; Lan, YB; Ding, SY; Yu, W; Wang, W. *Angew Chem Int Ed*, 2019, 58: 9443–9447; d) Biswal, BP; Vignolo-Gonzalez, HA; Banerjee, T; Grunenberg, L; Savasci, G; Gottschling, K; Nuss, J; Ochsenfeld, C; Lotsch, BV. *J Am Chem Soc*, 2019, 141: 11082–11092; e) Ding, J; Guan, X; Lv, J; Chen, X; Zhang, Y; Li, H; Zhang, D; Qiu, S; Jiang, H-L; Fang, Q. *J Am Chem Soc*, 2023, 145: 3248–3254.

4 a) Jhulki, S; Evans, AM; Hao, XL; Cooper, MW; Feriante, CH; Leisen, J; Li, H; Lam, D; Hersam, MC; Barlow, S; Bredas, JL; Dichtel, WR; Marder, SR. *J Am Chem Soc*, 2020, 142: 783–791; b) Yu, F; Liu, W; Li, B; Tian, D; Zuo, JL; Zhang, Q. *Angew Chem Int Ed*, 2019, 58: 16101–16104; c) Meng, Z; Stolz, RM; Mirica, KA. *J Am Chem Soc*, 2019, 141: 11929–11937; d) Das, G; Biswal, BP; Kandambeth, S; Venkatesh, V; Kaur, G; Addicoat, M; Heine, T; Verma, S; Banerjee, R. *Chem Sci*, 2015, 6: 3931–3939.

5 a) Martin-Illan, JA; Sierra, L; Ocon, P; Zamora, F. *Angew Chem Int Ed*, 2022, 61: e202213106; b) Keller, N; Bein, T. *Chem Soc Rev*, 2021, 50: 1813–1845; c) Ding, H; Li, J; Xie, G; Lin, G; Chen, R; Peng, Z; Yang, C; Wang, B; Sun, J; Wang, C. *Nat Commun*, 2018, 9: 5234; d) Jin, E; Asada, M; Xu, Q; Dalapati, S; Addicoat, MA; Brady, MA; Xu, H; Nakamura, T; Heine, T; Chen, Q; Jiang, D. *Science*, 2017, 357: 673–676.

6 Cote, AP; Benin, AI; Ockwig, NW; O'Keeffe, M; Matzger, AJ; Yaghi,

OM. Science, 2005, 310: 1166–1170.
7 a) Huang, S; Choi, JY; Xu, Q; Jin, Y; Park, J; Zhang, W. *Angew Chem Int Ed*, 2023, 62: e202303538; b) Liu, X; Li, J; Gui, B; Lin, G; Fu, Q; Yin, S; Liu, X; Sun, J; Wang, C. *J Am Chem Soc*, 2021, 143: 2123–2129; c) Zhu, Q; Wang, X; Clowes, R; Cui, P; Chen, L; Little, MA; Cooper, AI. *J Am Chem Soc*, 2020, 142: 16842v16848; d) Xie, Z; Wang, B; Yang, Z; Yang, X; Yu, X; Xing, G; Zhang, Y; Chen, L. *Angew Chem Int Ed*, 2019, 58: 15742–15746; e) Liu, W; Gong, L; Liu, Z; Jin, Y; Pan, H; Yang, X; Yu, B; Li, N; Qi, D; Wang, K; Wang, H; Jiang, J. *J Am Chem Soc*, 2022, 144: 17209–17218.
8 a) Xu, X; Cai, P; Chen, H; Zhou, HC; Huang, N. *J Am Chem Soc*, 2022, 144: 18511–18517; b) Liu, Y; Chen, P; Wang, Y; Suo, J; Ding, J; Zhu, L; Valtchev, V; Yan, Y; Qiu, S; Sun, J; Fang, Q. *Angew Chem Int Ed*, 2022, 61: e202203584; c) Gropp, C; Ma, T; Hanikel, N; Yaghi, OM. *Science*, 2020, 370: eabd6406; d) Liu, W; Wang, K; Zhan, X; Liu, Z; Yang, X; Jin, Y; Yu, B; Gong, L; Wang, H; Qi, D; Yuan, D; Jiang, J. *J Am Chem Soc*, 2023, 145: 8141–8149.
9 a) Wang, GB; Wang, YJ; Kan, JL; Xie, KH; Xu, HP; Zhao, F; Wang, MC; Geng, Y; Dong, YB. *J Am Chem Soc*, 2023, 145: 4951–4956; b) Zhou, ZB; Han, XH; Qi, QY; Gan, SX; Ma, DL; Zhao, X. *J Am Chem Soc*, 2022, 144: 1138–1143; c) Meng, F; Bi, S; Sun, Z; Wu, D; Zhang, F. *Angew Chem Int Ed*, 2022, 61: e202210447; d) Lei, Z; Wayment, LJ; Cahn, JR; Chen, H; Huang, S; Wang, X; Jin, Y; Sharma, S; Zhang, W. *J Am Chem Soc*, 2022, 144: 17737–17742; e) Feng, J; Zhang, YJ; Ma, SH; Yang, C; Wang, ZP; Ding, SY; Li, Y; Wang, W. *J Am Chem Soc*, 2022, 144: 6594–6603.
10 a) Zhou, Z; Zhang, L; Yang, Y; Vitorica-Yrezabal, IJ; Wang, H; Tan, F; Gong, L; Li, Y; Chen, P; Dong, X; Liang, Z; Yang, J; Wang, C; Hong, Y; Qiu, Y; Golzhauser, A; Chen, X; Qi, H; Yang, S; Liu, W; Sun, J; Zheng, Z. *Nat Chem*, 2023, 15: 841–847; b) Guan, Q; Zhou, LL; Dong, YB. *J Am Chem Soc*, 2023, 145: 1475–1496; c) Grunenberg, L; Savasci, G; Emmerling, ST; Heck, F; Bette, S; Cima Bergesch, A; Ochsenfeld, C; Lotsch, BV. *J Am Chem Soc*, 2023, DOI: 10.1021/jacs.3c02572; d) Zhou, ZB; Tian, PJ; Yao, J; Lu, Y; Qi, QY; Zhao, X. *Nat Commun*, 2022, 13: 2180; e) Ma, T; Kapustin, EA; Yin, SX; Liang, L; Zhou, Z; Niu, J; Li, LH; Wang, Y; Su, J; Li, J; Wang, X; Wang, WD; Wang, W; Sun, J; Yaghi, OM. *Science*, 2018, 361: 48–52; f) Evans, AM; Parent, LR; Flanders, NC; Bisbey, RP; Vitaku, E; Kirschner, MS; Schaller, RD; Chen, LX; Gianneschi, NC; Dichtel, WR. *Science*, 2018, 361: 52–57.
11 a) Vyas, VS; Haase, F; Stegbauer, L; Savasci, G; Podjaski, F; Ochsenfeld, C; Lotsch, BV. *Nat Commun*, 2015, 6: 8508; b) Gao, C; Li, J; Yin, S; Sun, J; Wang, C. *J Am Chem Soc*, 2020, 142: 3718–3723.
12 a) Wu, X; Han, X; Liu, Y; Liu, Y; Cui, Y. *J Am Chem Soc*, 2018, 140: 16124–16133; b) Wang, Y; Liu, Y; Li, H; Guan, X; Xue, M; Yan, Y; Valtchev, V; Qiu, S; Fang, Q. *J Am Chem Soc*, 2020, 142: 3736–3741.
13 Xie, Y; Li, J; Lin, C; Gui, B; Ji, C; Yuan, D; Sun, J; Wang, C. *J Am Chem Soc*, 2021, 143: 7279–7284.
14 a) Lanni, LM; Tilford, RW; Bharathy, M; Lavigne, JJ. *J Am Chem Soc*, 2011, 133: 13975–13983; b) Vazquez-Molina, DA; Pope, GM; Ezazi, AA; Mendoza-Cortes, JL; Harper, JK; Uribe-Romo, FJ. *Chem Commun*, 2018, 54: 6947–6950.
15 a) Auras, F; Ascherl, L; Hakimioun, AH; Margraf, JT; Hanusch, FC; Reuter, S; Bessinger, D; Doblinger, M; Hettstedt, C; Karaghiosoff, K; Herbert, S; Knochel, P; Clark, T; Bein, T. *J Am Chem Soc*, 2016, 138: 16703–16710; b) Bessinger, D; Ascherl, L; Auras, F; Bein, T. *J Am Chem Soc*, 2017, 139: 12035–12042; c) Jiang, G; Zou, W; Ou, Z; Zhang, L; Zhang, W; Wang, X; Song, H; Cui, Z; Liang, Z; Du, L. *Angew Chem Int Ed*, 2022, 61: e202208086.
16 a) Shao, P; Li, J; Chen, F; Ma, L; Li, Q; Zhang, M; Zhou, J; Yin, A; Feng, X; Wang, B. *Angew Chem Int Ed*, 2018, 57: 16501–16505; b) Chen, W; Wang, L; Mo, D; He, F; Wen, Z; Wu, X; Xu, H; Chen, L. *Angew Chem Int Ed*, 2020, 59: 16902–16909; c) He, T; Zhao, Z; Liu, R; Liu, X; Ni, B; Wei, Y; Wu, Y; Yuan, W; Peng, H; Jiang, Z; Zhao, Y. *J Am Chem Soc*, 2023, 145: 6057–6066.
17 a) Ghosh, S; Nakada, A; Springer, MA; Kawaguchi, T; Suzuki, K; Kaji, H; Baburin, I; Kuc, A; Heine, T; Suzuki, H; Abe, R; Seki, S. *J Am Chem Soc*, 2020, 142: 9752–9762; b) Fan, Y; Wen, Q; Zhan, TG; Qi, QY; Xu, JQ; Zhao, X. *Chem Eur J*, 2017, 23: 5668–5672.
18 Pang, ZF; Zhou, TY; Liang, RR; Qi, QY; Zhao, X. *Chem Sci*, 2017, 8: 3866–3870.
19 El-Mahdy, AFM; Kuo, C-H; Alshehri, A; Young, C; Yamauchi, Y; Kim, J; Kuo, S-W. *J Mater Chem A*, 2018, 6: 19532–19541.
20 Li, J; Zhang, H; Zhang, L; Wang, K; Wang, Z; Liu, G; Zhao, Y; Zeng, Y. *J Mater Chem A*, 2020, 8: 9523–9527.
21 Ascherl, L; Sick, T; Margraf, JT; Lapidus, SH; Calik, M; Hettstedt, C; Karaghiosoff, K; Döblinger, M; Clark, T; Chapman, KW; Auras, F; Bein, T. *Nat Chem*, 2016, 8: 310–316.
22 Kahveci, Z; Islamoglu, T; Shar, GA; Ding, R; El-Kaderi, HM. *CrystEngComm*, 2013, 15: 1524–1527.
23 Zhou, T-Y; Lin, F; Li, Z-T; Zhao, X. *Macromolecules*, 2013, 46: 7745–7752.
24 Diwakara, SD; Ong, WSY; Wijesundara, YH; Gearhart, RL; Herbert, FC; Fisher, SG; McCandless, GT; Alahakoon, SB; Gassensmith, JJ; Dodani, SC; Smaldone, RA. *J Am Chem Soc*, 2022, 144: 2468–2473.
25 Khayum, MA; Kandambeth, S; Mitra, S; Nair, SB; Das, A; Nagane, SS; Mukherjee, R; Banerjee, R. *Angew Chem Int Ed*, 2016, 55: 15604–15608.
26 Li, X; Xu, HS; Leng, K; Chee, SW; Zhao, X; Jain, N; Xu, H; Qiao, J; Gao, Q; Park, IH; Quek, SY; Mirsaidov, U; Loh, KP. *Nat Chem*, 2020, 12: 1115–1122.
27 Wang, K; Kang, X; Yuan, C; Han, X; Liu, Y; Cui, Y. *Angew Chem Int Ed*, 2021, 60: 19466–19476.
28 Albacete, P; Martinez, JI; Li, X; Lopez-Moreno, A; Mena-Hernando, SA; Platero-Prats, AE; Montoro, C; Loh, KP; Perez, EM; Zamora, F. *J Am Chem Soc*, 2018, 140: 12922–12929.
29 Yin, HQ; Yin, F; Yin, XB. *Chem Sci*, 2019, 10: 11103–11109.
30 Wang, X; Han, X; Zhang, J; Wu, X; Liu, Y; Cui, Y. *J Am Chem Soc*, 2016, 138: 12332–12335.
31 Zheng, Z; Yuan, C; Sun, M; Dong, J; Liu, Y; Cui, Y. *J Am Chem Soc*, 2023, 145: 6100–6111.
32 Jin, E; Fu, S; Hanayama, H; Addicoat, MA; Wei, W; Chen, Q; Graf, R; Landfester, K; Bonn, M; Zhang, KAI; Wang, HI; Mullen, K; Narita, A. *Angew Chem Int Ed*, 2022, 61: e202114059.
33 Shi, X; Yi, L; Deng, H. *Sci China Chem*, 2022, 65: 1315–1320.
34 a) Gui, B; Lin, G; Ding, H; Gao, C; Mal, A; Wang, C. *Acc Chem Res*, 2020, 53: 2225–2234; b) Ma, X; Scott, TF. *Commun Chem*, 2018, 1: 98.
35 Yan, S; Guan, X; Li, H; Li, D; Xue, M; Yan, Y; Valtchev, V; Qiu, S; Fang, Q. *J Am Chem Soc*, 2019, 141: 2920–2924.
36 a) El-Kaderi, HM; Hunt, JR; Mendoza-Cortes, JL; Cote, AP; Taylor, RE; O'Keeffe, M; Yaghi, OM. *Science*, 2007, 316: 268–272; b) Fang, Q; Gu, S; Zheng, J; Zhuang, Z; Qiu, S; Yan, Y. *Angew Chem Int Ed Engl*, 2014, 53: 2878–2882; c) Liu, Y; Ma, Y; Zhao, Y; Sun, X; Gandara, F; Furukawa, H; Liu, Z; Zhu, H; Zhu, C; Suenaga, K; Oleynikov, P; Alshammari, AS; Zhang, X; Terasaki, O; Yaghi, OM. *Science*, 2016, 351: 365–369; d) Lin, G; Ding, H; Yuan, D; Wang, B; Wang, C. *J Am Chem Soc*, 2016, 138: 3302–3305.
37 Jin, F; Lin, E; Wang, T; Geng, S; Wang, T; Liu, W; Xiong, F; Wang, Z; Chen, Y; Cheng, P; Zhang, Z. *J Am Chem Soc*, 2022, 144: 5643–5652.
38 Gong, C; Wang, H; Sheng, G; Wang, X; Xu, X; Wang, J; Miao, X; Liu, Y; Zhang, Y; Dai, F; Chen, L; Li, N; Xu, G; Jia, J; Zhu, Y; Peng, Y. *Angew Chem Int Ed*, 2022, 61: e202204899.
39 Liao, L; Guan, X; Zheng, H; Zhang, Z; Liu, Y; Li, H; Zhu, L; Qiu, S; Yao, X; Fang, Q. *Chem Sci*, 2022, 13: 9305–9309.
40 Guan, X; Ma, Y; Li, H; Yusran, Y; Xue, M; Fang, Q; Yan, Y; Valtchev, V; Qiu, S. *J Am Chem Soc*, 2018, 140: 4494–4498.
41 Ma, T; Li, J; Niu, J; Zhang, L; Etman, AS; Lin, C; Shi, D; Chen, P; Li, LH; Du, X; Sun, J; Wang, W. *J Am Chem Soc*, 2018, 140: 6763–6766.
42 Wu, C; Liu, Y; Liu, H; Duan, C; Pan, Q; Zhu, J; Hu, F; Ma, X; Jiu, T; Li, Z; Zhao, Y. *J Am Chem Soc*, 2018, 140: 10016–10024.

43 Xie, Y; Liu, M; Du, H; Gui, B; Sun, J; Wang, C. *Sci China Chem*, 2022, 65: 2177–2181.

Table of Contents graphic